Inorganic Chemistry
Article

Inorg. Chem. **2010**, *49*, 6697–6705 **6697**
DOI: 10.1021/ic100742c

$[Fe_4S_4]^q$ Cubane Clusters (q = 4+, 3+, 2+) with Terminal Amide Ligands

Christopher R. Sharp, Jeremiah S. Duncan,† and Sonny C. Lee*

Department of Chemistry, Princeton University, Princeton, New Jersey 08544 and Department of Chemistry, University of Waterloo, Waterloo, Ontario, Canada N2L 3G1. †Present address: Department of Atmospheric Science & Chemistry, Plymouth State University, Plymouth, NH 03264

Received April 19, 2010

Bis(trimethylsilyl)amide-ligated iron−sulfur cubane clusters $[Fe_4(\mu_3\text{-}S)_4(N\{SiMe_3\}_2)_4]^z$ (z = 0, 1−, 2−) are accessible by the reaction of $FeCl(N\{SiMe_3\}_2)_2(THF)$ (**1**) with 1 equiv of NaSH (z = 0), followed by reduction with either 0.25 (z = 1−) or 1 equiv (z = 2−) of Na_2S as needed. The anionic clusters are obtained as the sodium salts $[Na(THF)_2][Fe_4S_4(N\{SiMe_3\}_2)_4]$ and $[Na(THF)_2]_2[Fe_4S_4(N\{SiMe_3\}_2)_4]$; in the solid state, these two clusters both possess a unique contact ion pair motif in which individual sodium ions each coordinate to a cluster core sulfide, an adjacent amide nitrogen, and two THF donors. The monoanionic cluster can also be prepared as the lithium salt $[Li(THF)_4][Fe_4S_4(N\{SiMe_3\}_2)_4]$ by the reaction of **1** with 1:0.5 LiCl/Li_2S. The characterization of the three-membered redox series allows an analysis of redox trends, as well as a study of the effects of the amide donor environment on the $[Fe_4S_4]$ core. Bis(trimethylsilyl)amide terminal ligation significantly stabilizes oxidized cluster redox states, permitting isolation of the uncommon $[Fe_4S_4]^{3+}$ and unprecedented $[Fe_4S_4]^{4+}$ weak-field cores.

Introduction

The ligation of strongly basic nitrogen anions (N-anions) to weak-field iron−sulfur (Fe−S) clusters is a subject of growing interest in biological and synthetic inorganic chemistry. In the bioinorganic domain, N-anion donors are associated with two cluster types, the $[MoFe_7S_9Q]$ FeMo-cofactor and the $[Fe_8S_7]$ P-cluster (Chart 1), both found in the nitrogen-fixing MoFe protein of nitrogenase. For the FeMo-cofactor, the latest and highest resolution structural analysis has revealed an interstitial monatomic ligand (Q) at the center of the resting state cluster; the identity of Q is uncertain, but nitride is among the possible candidates.[1] Iron-bound N-anions also constitute plausible intermediates in a number of mechanistic conjectures for dinitrogen reduction by this cofactor.[2] For the P-cluster, deprotonated N-carboxamide ligation from the peptide backbone has been described in an oxidized (P^{OX}) state by macromolecular crystallography.[3] Both biometalloclusters are structurally and functionally complex, incompletely understood at the molecular level, and only partly accessible by chemical synthesis at present.[4]

From a strictly synthetic perspective, basic[5] N-anions present a relatively unexplored ligand environment in weak-field Fe−S chemistry that can lead to new clusters and reactivity. Chart 2 illustrates all presently known, structurally characterized types of synthetic weak-field, N-anion-ligated Fe−S clusters. (Given its dramatically different donor properties, the weakly basic azide ion is excluded as a ligand in this analysis.) For many years, the only member of this class was the pyrrolate-coordinated dinuclear cluster $[Fe_2(\mu\text{-}S)_2(NC_4H_4)_4]^{2-}$;[6] this general motif is gaining renewed, current interest via derivatives containing less basic monodentate and chelating N-heterocyclic anion ligands.[7] A second, isolated example is found in the ω-cyanoeneamido-ligated heterometallic cluster $[Tp_2Mo_2Fe_6(\mu_3\text{-}S)_6(\mu_4\text{-}S)_2(NHR)_4]^{4-}$ (Tp = hydrotris(pyrazolyl)borate;

*To whom correspondence should be addressed. E-mail: sclee@uwaterloo.ca.

(1) Einsle, O.; Tezcan, F. A.; Andrade, S.; Schmid, B.; Yoshida, M.; Howard, J. B.; Rees, D. C. *Science* **2002**, *297*, 1696.

(2) (a) Peters, J. W.; Szilagyi, R. K. *Curr. Opin. Chem. Biol.* **2006**, *10*, 101. (b) Seefeldt, L. C.; Dance, I. G.; Dean, D. R. *Biochemistry* **2004**, *43*, 1401.

(3) (a) Peters, J. W.; Stowell, M. H. B.; Soltis, S. M.; Finnegan, M. G.; Johnson, M. K.; Rees, D. C. *Biochemistry* **1997**, *36*, 1181. (b) Mayer, S. M.; Lawson, D. M.; Gormal, C. A.; Roe, S. M.; Smith, B. E. *J. Mol. Biol.* **1999**, *292*, 871.

(4) Seefeldt, L. C.; Hoffman, B. M.; Dean, D. R. *Annu. Rev. Biochem.* **2009**, *78*, 701.

(5) pK_a values for relevant protonated N-anion donors in organic solvents. (a) HN_3, 8 (DMSO); pyrrole, 23 (DMSO):Bordwell, F. G. *Acc. Chem. Res.* **1988**, *21*, 456. (b) $(Me_3Si)_2NH$, 26 (THF):Fraser, R. R.; Mansour, T. S.; Savard, S. *J. Org. Chem.* **1985**, *50*, 3232. (c) $H_2NC(Me)=CHCN$: We are unaware of a published pK_a value for this enamine; DFT calculations (B3LYP/6-31G(d), with MeCN and DMSO solvent reaction fields) suggest that the N-H acidity of the enamine is comparable to, but slightly higher than, that of pyrrole: Lee, S. C., unpublished results.

(6) (a) Coucouvanis, D.; Salifoglou, A.; Kanatzidis, M. G.; Simopoulos, A.; Papefthymiou, V. *J. Am. Chem. Soc.* **1984**, *106*, 6081. (b) Salifoglou, A.; Simopoulos, A.; Kostikas, A.; Dunham, R. W.; Kanatzidis, M. G.; Coucouvanis, D. *Inorg. Chem.* **1988**, *27*, 3394.

(7) (a) Ballmann, J.; Sun, X.; Dechert, S.; Schneider, B.; Meyer, F. *Dalton Trans.* **2009**, 4908. (b) Ballmann, J.; Albers, A.; Demeshko, S.; Dechert, S.; Bill, E.; Bothe, E.; Ryde, U.; Meyer, F. *Angew. Chem., Int. Ed.* **2008**, *47*, 9537. (c) Ballman, J.; Sun, X.; Dechert, S.; Bill, E.; Meyer, F. *J. Inorg. Biochem.* **2007**, *101*, 305.

Published on Web 06/16/2010

Chart 1. Biological Fe−S Clusters Ligated By N-Anions[a]

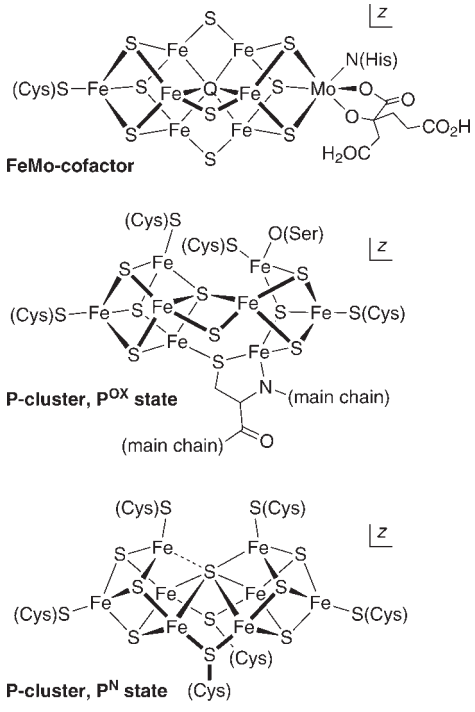

[a] Note: the P^N state is related to P^{OX} by 2-electron reduction; although it lacks N-anion ligands, the P^N structure is presented here for comparison with $Fe_8S_7(N\{SiMe_3\}_2)_4(tmtu)_2$ (Chart 2).

R = −C(Me)=CHCN);[8] the unusual coordinated N-anion in this system arises from self-condensation of MeCN solvent under very basic conditions. More recently, the bis(trimethylsilyl)amide ligand has emerged as a synthetically significant N-anion donor for weak-field Fe−S clusters. Its application has greatly expanded the range of N-anion-ligated cluster types to include the following:[9] *trans*-$Fe_2(\mu\text{-}S)_2(N\{SiMe_3\}_2)_2(tmtu)_2$ (tmtu = tetramethylthiourea);[10] $Fe_3(\mu_3\text{-}S)(\mu\text{-}SR)_3(N\{SiMe_3\}_2)_3$;[11] $[Fe_4(\mu_3\text{-}S)_4(N\{SiMe_3\}_2)_4]^z$ ($z = 0, 1-, 2-$);[10,12] $Fe_8(\mu_6\text{-}S)(\mu_3\text{-}S)_6(\mu\text{-}N\{SiMe_3\}_2)_2(N\{SiMe_3\}_2)_2(tmtu)_2$ and related terminal ligand-substituted derivatives;[13] and $Fe_8(\mu_6\text{-}S)(\mu_3\text{-}S)_6(\mu\text{-}N\{SiMe_3\}_2)(\mu\text{-}SR)_2(SR')_2$.[14] The last two cluster forms are particularly notable in possessing high-nuclearity $[Fe_8S_7]$ core frameworks that structurally resemble the biometalloclusters in the MoFe-protein; their existence connects this synthetic chemistry to biological systems and highlights the potential of N-anion ligands in the synthesis of novel Fe−S clusters.

We report here a full account of the preparation and characterization of the bis(trimethylsilyl)amide-ligated Fe−S cubane cluster $[Fe_4(\mu_3\text{-}S)_4(N\{SiMe_3\}_2)_4]^z$ in three redox states ($z = 0, 1-, 2-$). The $[Fe_4S_4]$ cubane core is a defining structural motif in Fe−S chemistry, and examples are known for a diverse array of capping ligands. This extensive, well-studied set of $[Fe_4S_4]$ derivatives provides a useful comparative database against which the intrinsic influence of the new bis(trimethylsilyl)amide environment can be discerned. The present account follows our initial disclosure of the existence of the three-membered redox series[12] and a subsequent, independent communication[10] of the $z = 0$ complex.

Results and Discussion

Syntheses. The syntheses of the $[Fe_4S_4]$ clusters described here originate from the mononuclear ferric precursor $FeCl(N\{SiMe_3\}_2)_2(THF)$ (**1**), which we have found previously to be a versatile starting material for the assembly of iron-imide clusters.[15] Complex **1**, prepared in high yield by reaction of $FeCl_3$ with 2 equiv of $NaN(SiMe_3)_2$ in tetrahydrofuran (THF; eq 1), offers several features that are attractive in cluster synthesis: (1) the hindered bis(trimethylsilyl)amide ligands offer steric control of the labile, reactive high-spin metal environment; (2) the heteroleptic environment allows different routes for derivatization, including substitution of the labile THF donor, anion metathesis of the bound chloride, and protolysis of the basic amide ligands; and, (3) with respect to N-anion ligated Fe−S cluster targets, the precursor is preorganized with the ligand functionality desired in the product. These considerations were applied in the stoichiometric reaction defined by eq 2.

$$FeCl_3 + 2Na[N(SiMe_3)_2] + THF(solvent) \rightarrow FeCl(N\{SiMe_3\}_2)_2(THF) + 2NaCl \quad (1)$$

$$4FeCl(N\{SiMe_3\}_2)_2(THF) + 4NaSH \rightarrow Fe_4(\mu_3\text{-}S)_4(N\{SiMe_3\}_2)_4 + 4HN(SiMe_3)_2 + 4NaCl + 4THF \quad (2)$$

Treatment of **1** with 1 equiv of NaSH affords the $Fe_4S_4(N\{SiMe_3\}_2)_4$ target (**2**) in high solution yield. The cluster self-assembly is quite selective and, by ^1H NMR assay, generates only one other paramagnetic species, a minority component (15:85 mol ratio vs **2**) isolated and identified as $[Na(THF)_2][Fe_4S_4(N\{SiMe_3\}_2)_4]$ (**3**). The principal product is neutral and extremely soluble in all common solvents, with evaporation of pentane solutions giving thick syrups rather than solid; sizable crystals (ca. 7 × 2 × 2 mm) can nevertheless be obtained on careful handling, although final isolated yields of pure **2** have been constrained in our hands by its high solubility. For preparative convenience, cluster **2** can be obtained directly from $FeCl_3$ in one pot, without loss in selectivity or yield, by sequential treatment with 2 equiv of $NaN(SiMe_3)_2$ in THF to generate **1** in situ, followed by 1 equiv of NaSH. Cluster **2** has also been reported from the

(8) Zhang, Y.; Holm, R. H. *Inorg. Chem.* **2004**, *43*, 674; the structure of the enamide ligand appears to be misassigned in this report as the iminate tautomer, $[N{=}C(Me)CH_2CN]^-$.

(9) Reference 8 also reports the existence of the bis(trimethylsilyl)amide-ligated cluster $Fe_8S_8(PCy_3)_4(N\{SiMe_3\}_2)_2$; no details were given, and the cluster is not included in Chart 2.

(10) Ohki, Y.; Sunada, Y.; Tatsumi, K. *Chem. Lett.* **2005**, *34*, 172.

(11) Pryadun, R.; Holm, R. H. *Inorg. Chem.* **2008**, *47*, 3366.

(12) Lee, S. C.; Holm, R. H. *Chem. Rev.* **2004**, *104*, 1135.

(13) (a) Ohki, Y.; Imada, M.; Murata, A.; Sunada, Y.; Ohta, S.; Honda, M.; Sasamori, T.; Tokitoh, N.; Katada, M.; Tatsumi, K. *J. Am. Chem. Soc.* **2009**, *131*, 13168. (b) Ohki, Y.; Murata, A.; Imada, M.; Tatsumi, K. *Inorg. Chem.* **2009**, *48*, 4271. (c) Ohki, Y.; Sunada, Y.; Honda, M.; Katada, M.; Tatsumi, K. *J. Am. Chem. Soc.* **2003**, *125*, 4052–4053.

(14) Ohki, Y.; Ikagawa, Y.; Tatsumi, K. *J. Am. Chem. Soc.* **2007**, *129*, 10457.

(15) (a) Duncan, J. S.; Zdilla, M. J.; Lee, S. C. *Inorg. Chem.* **2007**, *41*, 1071. (b) Duncan, J. S.; Nazif, T. M.; Verma, A. K.; Lee, S. C. *Inorg. Chem.* **2003**, *42*, 1211.

Chart 2. Synthetic Weak-Field Fe−S Clusters Ligated by N-Anions

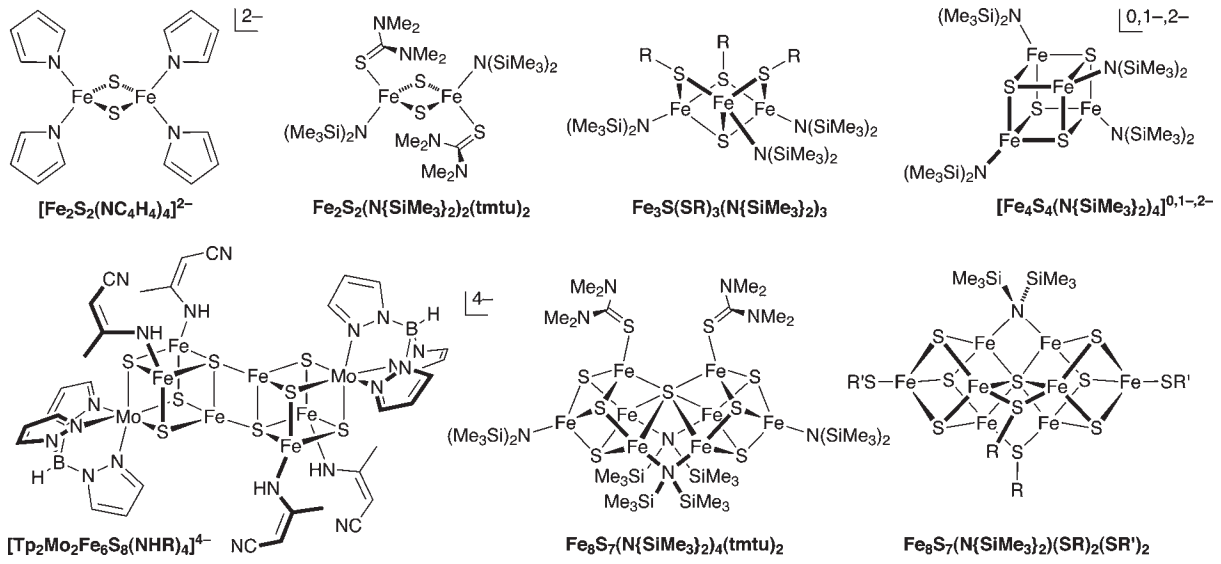

reaction of the ferrous amide complex $Fe(N\{SiMe_3\}_2)_2$[16] with 1 equiv of elemental sulfur,[10] although this preparation appears to be complicated by its imbalanced stoichiometry and by the formation of $Fe(N\{SiMe_3\}_2)_3$[17] as a coproduct.

The minority product **3** is the one-electron reduced form of **2** and likely forms through the reduction of **2** by unreacted hydrosulfide. We can exploit this redox behavior synthetically: thus, addition of 0.25 equiv of Na_2S to the 1:1 reaction system of **1** and NaSH cleanly shifts the ratio of **2**/**3** to 1:9 in favor of **3**. The reduction chemistry can be driven further, with addition of 1 equiv of Na_2S to the 1:1 reaction system leading to the cubane dianion, isolated as $[Na(THF)_2]_2[Fe_4S_4(N\{SiMe_3\}_2)_4]$ (**4**). Our empirically derived reductant stoichiometries suggest that disulfide ($[S_2]^{2-}$) is the oxidized product in the synthesis of **3** and that reductant is in excess for the formation of **4**. However, given the heterogeneous nature of the reaction system and the small amounts employed, we are cautious in treating our stoichiometries as limiting for balanced reactions. In principle, a soluble one-electron reductant of appropriate potential could be used to accomplish the reductions precisely; in practice, Na_2S is convenient and effective. The reaction of **1** with NaSH, followed, as needed, by addition of Na_2S reductant, therefore provides simple, efficient access to three separate redox states of the amide-ligated $[Fe_4S_4]$ core.

Reactions of **1** with sulfide (Li_2S or Na_2S) were also screened in an effort to obtain other amide-ligated Fe−S clusters. These attempts yielded poorly separable product mixtures that contain $Fe(N\{SiMe_3\}_2)_3$[17] and amide-ligated cubane species (identified by crystallography and ^1H NMR spectroscopy, respectively), as well as unknown NMR-active paramagnetic species. The contrast between these reaction outcomes relative to those in the hydrosulfide chemistry underscores the importance of the balanced stoichiometry provided by eq 2 for the selective assembly of the $[Fe_4S_4]$ core from precursor **1**. The sulfide-only reaction systems will not be discussed further in this report, except to note the isolation and crystallographic characterization of the monolithium cubane salt $[Li(THF)_4][Fe_4S_4(N\{SiMe_3\}_2)_4]$ (**5**) from the reaction of **1** with 1:0.5 $LiCl/Li_2S$ in THF. The structure of **5** is relevant in the next section for comparison against that of the isoelectronic sodium-associated cluster **3**.

Structures. Single crystal X-ray diffraction analyses establish the existence of $[Fe_4S_4]$ clusters in compounds **2**−**5** (Figure 1, Tables 1−4). One entire cluster is contained within the asymmetric units of crystalline **2** and **3**, while two independent half-clusters and a single quarter-cluster make up the asymmetric units of **4** and **5**, respectively, with complete clusters generated by crystallographic 2-fold rotation and 4-fold rotoinversion symmetry. The crystal structure of **2** has been reported independently elsewhere;[10] for comparative purposes, we present here a separate structure determination for this compound.

(i) General Cluster Structures. As expected for the cluster type, each $[Fe_4S_4]$ cubane core comprises concentric, interpenetrating Fe_4 and S_4 tetrahedra with nonplanar Fe_2S_2 rhombic faces. Terminal ligation is provided by bis(trimethylsilyl)amides; the amide nitrogens are planar, with the exceptions of a single amide in **2** and the unique amide in **5**, both of which exhibit modest pyramidalization of unknown origin, as well as the sodium-coordinated amides described below.

(ii) Cation Interactions. The lithium cation in the structure of **5** occurs as a separated, tetrahedrally solvated $[Li(THF)_4]^+$ unit and is unexceptional. By contrast, the sodium ions in the structures of **3** and **4** share a distinctive, unique structural motif involving close cation interaction along a cluster core edge. The coordination sphere about the individual sodium centers is highly distorted 4-coordinate, with an approximately T-shaped donor plane of core sulfide, amide nitrogen, and THF oxygen, plus a fourth THF donor ligated obliquely off-plane and at a longer distance; an additional close contact also exists with a silylmethyl group. The sodium-amide interaction pyramidalizes the nitrogen atom toward the coordinated

(16) Andersen, R. A.; Faegri, K., Jr.; Green, J. C.; Haaland, A.; Lappert, M.; Leung, W.-P.; Rypdal, K. *Inorg. Chem.* **1988**, *27*, 1782.

(17) (a) Hursthouse, M. B.; Rodesiler, P. F. *J. Chem. Soc., Dalton Trans.* **1972**, 2100. (b) Bradley, D. C.; Hursthouse, M. B.; Rodesiler, P. F. *Chem. Commun.* **1969**, 14.

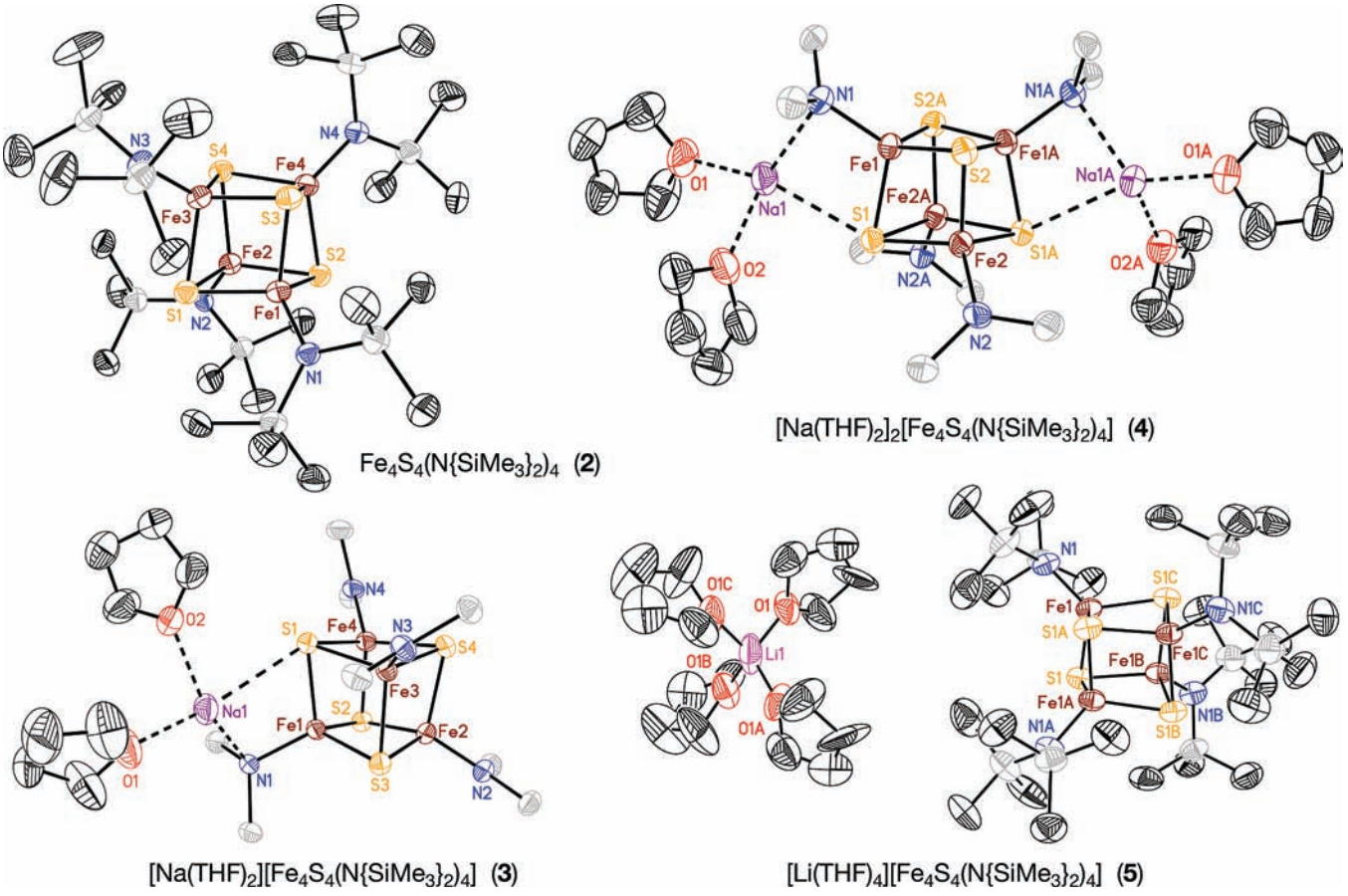

Figure 1. Structures of $Fe_4S_4(N\{SiMe_3\}_2)_4$ (**2**, top left), $[Na(THF)_2][Fe_4S_4(N\{SiMe_3\}_2)_4]$ (**3**, bottom left), $[Na(THF)_2]_2[Fe_4S_4(N\{SiMe_3\}_2)_4]$ (**4**, top right), and $[Li(THF)_4][Fe_4S_4(N\{SiMe_3\}_2)_4]$ (**5**, bottom right) with thermal ellipsoids (50% probability level) and selected atom labels. For clarity, hydrogen atoms are not shown, and silicon methyl substituents were omitted in the depictions of **3** and **4**. For **4** and **5**, atoms with labels ending in letters ("A", "B", or "C") were generated by crystallographic 2-fold rotation or 4-fold rotoinversion symmetry, respectively. Only one of two independent clusters is shown in the structure of **4**.

Table 1. Selected Distances (Å) and Angles (deg) for $Fe_4S_4(N\{SiMe_3\}_2)_4$ (**2**)[a]

	n[b]	mean of n[c]	range[d]
Fe−S (short)	4	2.272(12)	2.2544(15)−2.2815(15)
Fe−S (long)	8	2.308(9)	2.2972(14)−2.3177(14)
Fe−S (all)	12	2.30(2)	
Fe−N	4	1.864(5)	1.858(4)−1.871(4)
Fe···Fe (short)	2	2.872(2)	2.8707(10), 2.8740(10)
Fe···Fe (long)	4	2.93(6)	2.8864(9)−3.0047(9)
Fe···Fe (all)	6	2.91(5)	
S···S (short)	4	3.50(3)	3.4629(18)−3.5351(17)
S···S (long)	2	3.556(11)	3.548(2), 3.563(2)
S···S (all)	6	3.52(4)	
S−Fe−S	12	100.1(18)	96.76(5)−101.86(5)
N−Fe−S	12	117(4)	110.09(12)−124.69(12)
N2 planarity[e]	1	0.204(4)	
N planarity[e] (others)	3	0.031(6)	0.027(4)−0.038(4)

[a] Entries are sorted according to the idealized D_{2d} distortion noted in the text, with the principal axis oriented approximately parallel to the short Fe1−S1, Fe2−S2, Fe3−S3, and Fe4−S4 bonds (Figure 1); a full listing of metrics is available in CIF format as Supporting Information. [b] Number of independent values corresponding to the metric type. [c] Arithmetic mean, with uncertainty representing the standard deviation from the mean. [d] Range of independent values. [e] Planarity is measured by the perpendicular displacement of the designated atom from the plane of the relevant directly bonded atoms (for N: Fe, Si, Si).

cation and lengthens the adjoining Fe−N bond. Sodium cation coordination with terminal ligands and core sulfides has been proposed to accelerate terminal ligand substitution in Fe−S clusters;[18] in this context, the Fe−N bond

(18) Henderson, R. A. *J. Chem. Soc., Dalton Trans.* **1999**, 119.

Table 2. Selected Distances (Å) and Angles (deg) for $[Na(THF)_2][Fe_4S_4(N\{SiMe_3\}_2)_4]$ (**3**)[a]

	n[b]	mean of n[c]	range[d]
Fe−S	12	2.292(19)	2.2625(10)−2.3174(10)
Fe1−N1	1	1.945(3)	
Fe−N (others)	3	1.892(2)	1.890(3)−1.894(3)
Fe−N (all)	4	1.91(3)	
Fe···Fe	6	2.87(4)	2.8361(7)−2.9203(7)
S···S	6	3.54(4)	3.5076(12)−3.6117(13)
S−Fe−S	12	101.2(15)	98.76(4)−104.51(4)
N−Fe−S	12	117(3)	112.25(9)−121.26(9)
N1 planarity[e]	1	0.370(3)	
N planarity[e] (others)	3	0.06(2)	0.040(3)−0.088(3)

Cation-Associated Metrics

Na1···N1	2.533(3)	Na1···O1	2.269(3)
Na1···S1	3.093(2)	Na1···O2	2.315(3)
Na1···C16	3.031(4)	Na1 planarity[e]	0.081(3)
O2 displacement[f]		1.371(5)	

[a] A full listing of metrics is available in CIF format as Supporting Information. [b] Number of independent values corresponding to the metric type. [c] Arithmetic mean, with uncertainty representing the standard deviation from the mean. [d] Range of independent values. [e] Planarity is measured by the perpendicular displacement of the designated atom from the plane of the relevant directly bonded atoms (for N: Fe, Si, Si; for Na1: N1, S1, O1). [f] Perpendicular displacement from the plane of N1, S1, O1.

Table 3. Selected Distances (Å) and Angles (deg) for $[Na(THF)_2]_2[Fe_4S_4(N\{SiMe_3\}_2)_4]$ (**4**)[a]

	n[b]	mean of n[c]	range[d]
Fe−S (short)	4	2.279(6)	2.273(2)−2.286(2)
Fe−S (long)	8	2.320(8)	2.310(2)−2.331(2)
Fe−S (all)	12	2.31(2)	
Fe−N (short)	2	1.932(3)	1.929(6), 1.934(6)
Fe−N (long)	2	1.978(−)	1.978(6), 1.978(6)
Fe−N (all)	4	1.95(3)	
Fe···Fe (short)	2	2.79(2)	2.779(2), 2.802(2)
Fe···Fe (long)	6	2.881(6)	2.8726(15)−2.8898(15)
Fe···Fe (all)	8	2.86(4)	
S···S (long)	4	3.65(2)	3.634(4)−3.680(4)
S···S (short)	4	3.538(11)	3.524(3)−3.549(3)
S···S (all)	8	3.60(6)	
S−Fe−S	12	101.7(18)	99.69(8)−105.46(7)
N−Fe−S	12	116(4)	112.9(2)−122.3(2)
N1, N3 planarity[e]	2	0.052(13)	0.043(7), 0.061(7)
N2, N4 planarity[e]	2	0.31(1)	0.302(6), 0.316(6)

Mean Cation-Associated Metrics[c,f]

Na···N	2.55(3)	Na···O (short)	2.28(2)
Na···S	2.97(3)	Na···O (long)	2.343(6)
Na···C[g]	3.17(5)	Na planarity[e]	0.21(6)
O(long) displacement[h]		1.83(10)	

[a] Entries are sorted according to the idealized distortions noted in the text, with the principal axes for the two independent clusters oriented approximately parallel to the short Fe1−S1 and Fe2−S2 (cluster 1, Figure 1), or Fe3−S3 and Fe4−S4 bonds (cluster 2); a full listing of metrics is available in CIF format as Supporting Information. [b] Number of independent values corresponding to the metric type. [c] Arithmetic mean, with uncertainty representing the standard deviation from the mean. [d] Range of independent values. [e] Planarity is measured by the perpendicular displacement of the designated atom from the plane of the relevant directly bonded atoms (for N: Fe, Si, Si; for Na: N, S, O(short)). [f] Mean values for two independent sodium cations. [g] Nearest methyl carbons (C11A, C22). [h] Perpendicular displacement from the plane of N, S, O(short).

elongation found here can be taken as evidence of ground-state labilization by sodium coordination. Sodium cation interactions with Fe−S clusters have been directly observed in a few prior instances,[19] but these cases all involve cation chelation by multiple core sulfides rather than the sulfide/terminal ligand binding mode observed here. Inasmuch as both sodium salts are soluble in *n*-pentane, tight ion pairing appears to be retained in some form in solution as well.

(iii) Core Distortions. Weak-field $[Fe_4S_4]$ cluster cores often exhibit small, systematic distortions away from idealized T_d symmetry.[20] The most common deformation mode is an approximate D_{2d} distortion characterized primarily by the existence of four "short" and eight "long" Fe−S distances parallel and perpendicular, respectively, to the S_4 axis of the point group, with other core metrics segregating per this distortion symmetry. This distortion is found across a range of cluster redox states and is particularly well-recognized in the extensively studied $[Fe_4S_4]^{2+}$ core oxidation state. Its origin is not fully understood, although interionic interactions and packing considerations have recently been proposed as major factors in the distortion of $[Fe_4S_4]^{+}$ systems.[21]

Table 4. Selected Distances (Å) and Angles (deg) for $[Li(THF)_4][Fe_4S_4(N\{SiMe_3\}_2)_4]$ (**5**)[a]

Fe1−S1	2.277(2)	Fe1···Fe1A	2.8511(14)
Fe1−S1A	2.2969(14)	Fe1···Fe1B	2.9049(14)
Fe1−S1B	2.307(2)	mean of Fe···Fe	2.88(4)
mean[b] of Fe−S (long)	2.302(7)	S1···S1A	3.557(3)
mean of Fe−S (all)	2.294(15)	S1···S1B	3.524(3)
Fe1−N1	1.912(5)	mean of S···S	3.54(2)
N1 planarity[c]	0.163(5)	Li1···O[b,d]	1.951(14)

	n[e]	mean of n[b]	range[f]
S−Fe−S	3	100.8(11)	99.88(6)−102.09(5)
N−Fe−S	3	117(3)	114.36(15)−120.76(16)

[a] Entries are sorted according to the idealized D_{2d} distortion noted in the text, with the principal axis oriented approximately parallel to the short Fe1−S1 bond (Figure 1); a full listing of metrics is available in CIF format as Supporting Information. [b] Arithmetic mean, with uncertainty representing the standard deviation from the mean. [c] Planarity is measured by the perpendicular displacement of the designated atom from the plane of the relevant directly bonded atoms (for N: Fe, Si, Si). [d] Mean of two disordered THF oxygen positions. [e] Number of independent values corresponding to the metric type. [f] Range of independent values.

Similar D_{2d} distortions exist for the well-isolated clusters in the structures of **2** and **5**. The deformations, which occur here in the $[Fe_4S_4]^{4+}$ and $[Fe_4S_4]^{3+}$ core states, are entirely comparable in degree to those found in other ligand systems and redox states, although the specifics of the distortions vary. In **2**, the core distortion is marked by compression of the Fe_4 tetrahedron and elongation of the S_4 tetrahedron along the idealized S_4 axis, whereas in **5**, the opposite is found; for the majority of $[Fe_4S_4(SR)_4]^{2-}$ systems, the Fe_4 and S_4 tetrahedra both compress. More complicated core deformations are found in the sodium-coordinated clusters of **3** and **4**, likely because of the influence of the tight cation-cluster interactions. In **4**, both independent cluster cores distort to four parallel short and eight long Fe−S distances per core; however, the overall distortion better idealizes to C_{2v} symmetry, as only one distinctly short Fe···Fe contact occurs in each core. The T_d-averaged core metrics in cation-coordinated **4**, however, do not differ appreciably from those found in the isolated isoelectronic cluster of **5**. For **3**, no systematic deformation mode is evident.

(iv) Redox Trends and Comparison with Other $[Fe_4S_4]$ Systems. The structural effect of cluster oxidation state is most evident in the mean Fe−N distances, which increase progressively upon reduction as expected from ionic radii considerations. For averaged core metrics, oxidation state dependencies are more subtle, with Fe···Fe contacts decreasing and S···S contacts increasing upon reduction, while Fe−S distances behave inconsistently. The magnitudes of the metrical variations in the present redox series are comparable to those found in other $[Fe_4S_4]$ systems where multiple redox states have been structurally characterized,[22] although individual redox-correlated trends are not entirely consistent between

(19) (a) Hong, D.; Zhang, Y.; Holm, R. H. *Inorg. Chim. Acta* **2005**, *358*, 2303. (b) You, J.-F.; Papaefthymiou, G. C.; Holm, R. H. *J. Am. Chem. Soc.* **1992**, *114*, 2697. (c) You, J.-F.; Snyder, B. S.; Papaefthymiou, G. C.; Holm, R. H. *J. Am. Chem. Soc.* **1990**, *112*, 1067. (d) You, J.-F.; Snyder, B. S.; Holm, R. H. *J. Am. Chem. Soc.* **1988**, *110*, 6589. (e) Strasdeit, H.; Krebs, B.; Henkel, G. *Inorg. Chem.* **1984**, *23*, 1816.

(20) (a) Rao, P. V.; Holm, R. H. *Chem. Rev.* **2004**, *104*, 527. (b) Berg, J. M.; Holm, R. H. In *Iron-Sulfur Proteins*; Spiro, T. G., Ed.; Wiley: New York, 1982; Chapter 1.

(21) Hagen, K. S.; Uddin, M. *Inorg. Chem.* **2008**, *47*, 11807.

(22) (a) *Cambridge Structural Database*, version 5.31; Cambridge University: Cambridge, England, February 2010. (b) Allen, F. H. *Acta Crystallogr.* **2002**, *B58*, 380.

Table 5. Weak-Field $[Fe_4S_4L_4]^z$ Clusters[a] Isolated in Multiple Redox States

L[a]	z	q[b]	ref.
$N(SiMe_3)_2$	2−/1−/0	2+/3+/4+	this work
SH	3−/2−	1+/2+	20a
SAlk[c]	3−/2−	1+/2+	20a
SAr[c]	3−/2−/1−	1+/2 + 3+	20a
Cl	3−/2−	1+/2+	21,25
CN	4−/3−	0/1+	26

[a] L restricted to monodentate terminal ligands. [b] q = core oxidation state, $[Fe_4S_4]^q$. [c] Alk = alkyl, Ar = aryl.

systems. In general, the changes in core metrics are minor throughout, and the $[Fe_4S_4]$ cubane geometry appears relatively insensitive to changes in redox state.

The influence of the amide ligation can be analyzed at parity of core oxidation and cluster charge states by comparing **4** with the sizable set of $[Fe_4S_4X_4]^{2-}$ (X = halide, thiolate) systems.[22,23] The average iron coordination environment in **2** presents compressed S−Fe−S angles and slightly longer Fe−S bonds relative to these reference sets. The S−Fe−S angular compression can be ascribed to steric repulsion between the hindered bis(trimethylsilyl)amide ligand and the core sulfides; if we assume that Fe−S bond lengths are relatively constant, the S−Fe−S angular compression leads directly to the observed trends in Fe···Fe and S···S contacts, which are longer and shorter, respectively, than those of $[Fe_4S_4X_4]^{2-}$ clusters. Comparison at higher oxidation states is confined to a single example at the +3 core oxidation state ($[Fe_4S_4(SAr)_4]^-$, Ar = 2,4,6-triisopropylphenyl),[24] where the same differences exist. The steric influence of the hindered amide also seems discernible across the present redox series and correctly accounts for the trends already noted: as Fe−N bond lengths decrease with increasing oxidation state, steric repulsion increases; this compresses S−Fe−S angles further, leading to longer Fe···Fe and shorter S···S contacts.

Redox Properties. The accessibility of multiple redox states is a prominent feature of the $[Fe_4S_4]$ motif. For all known weak-field $[Fe_4S_4L_4]^z$ species, where L is a monodentate terminal ligand, clusters have been isolated in more than one core oxidation state for a number of ligand classes (Table 5).[22] Of these, however, only arylthiolate-ligated species have been structurally characterized in three separate oxidation states prior to the present report.[20a,22]

The amide-ligated redox series was defined through electrochemical studies (Table 6). The cyclic voltammogram of doubly reduced cluster **4** (Figure 2) establishes two oxidative processes, corresponding to the z = 2−/1− and 1−/0 redox couples, with no other well-defined states accessible under the measurement conditions. The 2−/1− oxidation is chemically reversible (peak current ratio = $i_{pa}/i_{pc} \approx 1$), although subject to slow electron transfer kinetics as indicated by a relatively large separation of peak potentials (ΔE_p) that increases with increasing scan rate (v). The 1−/0 response more closely approaches electrochemical reversibility: $i_{pa}/i_{pc} \approx 1$ for v = 10 to 750 mV/s, $E_{1/2}$ and ΔE_p are largely independent of v, and a plot of i_p versus $v^{1/2}$ is linear with a near-zero intercept.[27] The reversibility of the 1−/0 couple, however, is contingent on the addition of benzene to the 0.1 M (n-$Bu_4N)ClO_4$ (TBAP)/MeCN electrolyte solution (ca. 1:9 v/v); without the benzene co-solvent, we observe irreversible behavior that may reflect electrodeposition of the neutral cluster from the polar medium. The use of the benzene/MeCN solvent mixture otherwise does not appear to affect redox properties appreciably relative to measurement in pure MeCN solvent, as demonstrated by near identical 2−/1− potentials and curve shapes between the two solvent systems. Voltammograms for the mono-reduced and neutral cubanes (not shown) exhibit features identical to those obtained for **4**; as expected, the equilibrium potential occurs between the two redox processes for **3** and on the oxidized side of both processes for **2**, thereby confirming the assignment of the redox couples.

Table 6. Chemically Reversible Redox Couples ($E_{1/2}$) for Selected $[Fe_4S_4X_4]^z$ Clusters (V vs. SCE)

X	solvent	z = 4−/3−	3−/2−	2−/1−	1−/0	ref.
$N(SiMe_3)_2$	MeCN			−0.51	+0.37	this work
S^{t}Bu	MeCN		−1.33	−0.15		28
S^{t}Bu	CH_2Cl_2		−1.44	−0.19		28
S^{t}Bu	DMF	−2.16	−1.42	−0.14		29
SPh	MeCN	−1.72	−1.00			30a
SPh	CH_2Cl_2		−1.00	0.14		28
SAr*[a]	CH_2Cl_2		−1.20	−0.12		24
Cl	MeCN		−0.79			25

[a] Ar* = 2,4,6-triisopropylphenyl.

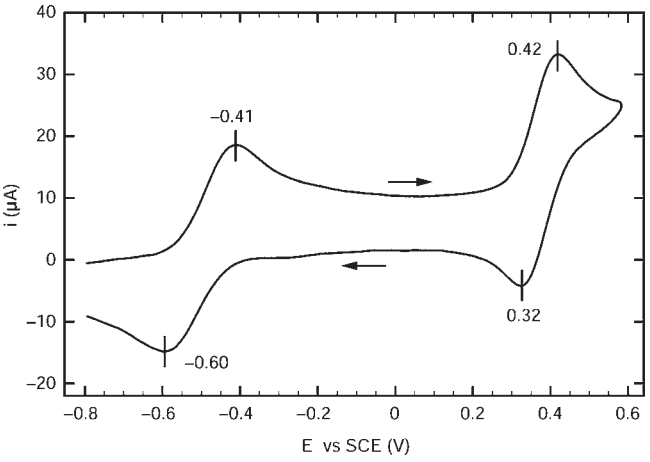

Figure 2. Cyclic voltammogram of $[Na(THF)_2]_2[Fe_4S_4(N\{SiMe_3\}_2)_4]$ (**4**) (0.1 M TBAP in 1:9 v/v benzene/MeCN, 100 mV/s). Peak potentials vs SCE are indicated.

(23) From reference 22, mean metrics and standard deviations for selected core metrics of $[Fe_4S_4X_4]^{2-}$clusters, X = Cl/SAr/SAlk: Fe−S, 2.287(13)/2.281(19)/2.29(3); Fe···Fe, 2.771(15)/2.735(18)/2.75(2); S···S, 3.59(2)/3.60(3)/3.61(4); S−Fe−S, 103.5(6)/104.2(8)/104.1(11); number of observations, 5/9/17.

(24) O'Sullivan, T.; Millar, M. M. *J. Am. Chem. Soc.* **1985**, *107*, 4096.
(25) Wong, G. B.; Bobrik, M. A.; Holm, R. H. *Inorg. Chem.* **1978**, *17*, 578.
(26) (a) Scott, T. A.; Berlinguette, C. P.; Holm, R. H.; Zhou, H.-C. *Proc. Natl. Acad. Sci. U.S.A.* **2005**, *102*, 9741. (b) Scott, T. A.; Zhou, H.-C. *Angew. Chem., Int. Ed.* **2004**, *43*, 5628.
(27) Bard, A. J.; Faulkner, L. R. *Electrochemical Methods: Fundamentals and Applications*; Wiley: New York, 2001; Chapter 6.
(28) Blonk, H. L.; Kievet, O.; Roth, E. K.-H.; Jordanov, J.; van der Linden, J. G. M.; Steggerda, J. A. *Inorg. Chem.* **1991**, *30*, 3231.
(29) Mascharak, P. K.; Hagen, K. S.; Spence, J. T.; Holm, R. H. *Inorg. Chim. Acta* **1983**, *80*, 157.
(30) (a) Cambray, J.; Lane, R. W.; Wedd, A. G.; Johnson, R. W.; Holm, R. H. *Inorg. Chem.* **1977**, *16*, 2565. (b) DePamphilis, B. V.; Averill, B. A.; Herskovitz, T.; Que, L., Jr.; Holm, R. H. *J. Am. Chem. Soc.* **1974**, *96*, 4160.

Table 7. Spectroscopic Data for $[Fe_4S_4(N\{SiMe_3\}_2)_4]^z$ ($z = 0, 1-, 2-$) Clusters

	electronic absorption:[a] λ, nm (ε_M, L mol^{-1} cm^{-1})	^{1}H NMR:[b] δ, ppm	Mössbauer:[c] δ ($\lvert\Delta E_Q\rvert$), mm/s
$Fe_4S_4(N\{SiMe_3\}_2)_4$ (**2**)	231 (19,900), 268 (21,900), 449 (19,400)	2.40 (br)	0.26 (1.67)
$[Na(THF)_2][Fe_4S_4(N\{SiMe_3\}_2)_4]$ (**3**)	257 (22,900), 404 (17,700), 630 (sh, 2400)	1.3 (THF, 4H), 1.60 (br, 72H), 3.2 (THF, 4H)	0.33 (1.35)[d]
$[Na(THF)_2]_2[Fe_4S_4(N\{SiMe_3\}_2)_4]$ (**4**)	249 (25,600), 350 (15,400), 685 (1900)	1.07 (br, 72H), 1.3 (THF, 8H), 3.3 (THF, 8H)	0.45 (1.30)

[a] THF solution, about 22 °C. [b] C_6D_6 solution, about 22 °C. [c] Isomer shifts measured at 4.2 K, referenced to Fe metal at room temperature; errors in fit estimated at 0.02 mm/s. [d] The broad doublet at 4.2 K sharpens to two superimposed, equal-intensity doublets at 150 K: 0.27 (1.28), 0.36 (1.00).

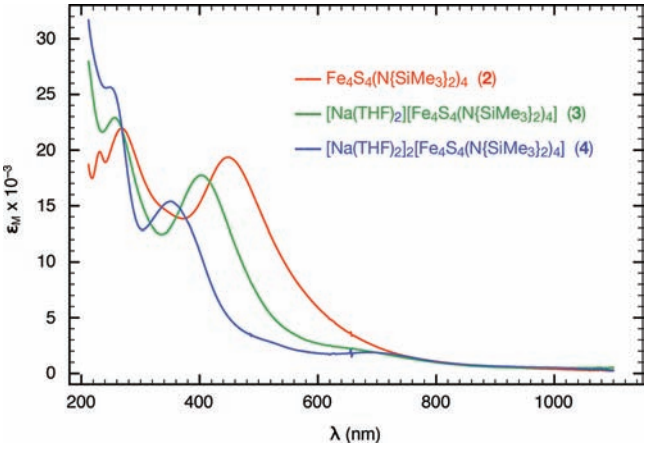

Figure 3. UV−visible absorption spectra of $Fe_4S_4(N\{SiMe_3\}_2)_4$ (**2**), $[Na(THF)_2][Fe_4S_4(N\{SiMe_3\}_2)_4]$ (**3**), and $[Na(THF)_2]_2[Fe_4S_4(N\{SiMe_3\}_2)_4]$ (**4**) in benzene.

Bis(trimethylsilyl)amide ligation thermodynamically stabilizes oxidized states relative to thiolate-ligated analogues. The greater intrinsic electron donor capacity of the amide ligand is evident in comparing redox potentials (Table 6), which show the progression $(Me_3Si)_2N^- < {}^tBuS^- < PhS^-$ at equivalent couples. In contrast to thiolate systems, the amide environment does not allow access to reduced $[Fe_4S_4]^{1+,0}$ core states under our measurement conditions, but instead provides both electrochemical and synthetic entry to oxidized clusters, including the all-ferric $[Fe_4S_4]^{4+}$ core that is unknown in any other weak-field ligand set. With thiolate ligands, stabilization of even the $[Fe_4S_4]^{3+}$ core is difficult, requiring the use of hindered thiolates and solvents of low nucleophilicity, and only one physically isolated example has been reported.[24] Accordingly, it seems likely that the steric shielding afforded by the trimethylsilyl substituents and the oxidative stability of the amide ligands themselves also contribute to the stabilization of oxidized cores in the present system.

Solution Identification. The different members of the redox series are readily distinguished in solution by ^{1}H NMR spectroscopy (Table 7). All of the cluster forms display only one signal for the trimethylsilyl group, indicating site equivalence on the spectroscopic time scale; cluster paramagnetism places this resonance at a chemical shift that is specific for each redox state and significantly downfield of the diamagnetic signal positions of both $HN(SiMe_3)_2$ and $NaN(SiMe_3)_2$ (0.10 and 0.12 ppm in C_6D_6, respectively). The spectra of the anionic clusters also show signals for cation-associated THF that integrate to the stoichiometries determined in the solid state by crystallographic and elemental analyses.

The electronic absorption spectra are also characteristic (Figure 3, Table 7). The three members of the redox series show optical spectra dominated by intense features that are almost certainly ligand-to-metal charge transfer (LMCT) in origin. The overall appearance of all three cluster spectra are comparable despite the changes in electron count, with a hypsochromic shift evident, particularly for the lowest energy transition, upon reduction. The lowest energy transition occurs in the visible range, and the reductive blue shift therefore results in a discernible change in hue for the deeply colored solutions, from red-black for **2** to yellow-black for **3** and green-black for **4**. A similar band pattern and reductive blue shift also exists in thiolate-ligated cubane systems.[24,30] In comparing systems with isoelectronic cores, the lowest energy transitions define a qualitative optical electronegativity series $(Me_3Si)_2N^- > ArO^- > AlkS^- > ArS^-$.[30,31] This behavior can be rationalized by viewing LMCT transitions as internal redox reactions: the increased donor capacity and chemical electronegativity of the amide ligand destabilize metal reduction and terminal ligand oxidation, respectively, thereby shifting LMCT processes to higher energies relative to thiolate and aryloxide systems. We acknowledge, however, that this comparison is imperfect because of the different solvents used in the various systems and the tight ion pairing present in **3** and **4**.

Other Properties. Variable temperature magnetic susceptibility measurements on polycrystalline samples reveal similar behavior for the even-electron clusters **2** and **4**. Both show susceptibilities that decrease with temperature, reach a minimum at about 50 K (**2**: 0.66 μ_B at 51 K; **4**: 0.56 μ_B at 46 K), then rise as absolute zero is approached (plots provided as Supporting Information). This behavior is known for thiolate, phenoxide, and chloride ligated $[Fe_4S_4]^{2+}$ systems and has been treated in detail elsewhere.[31,32] The low susceptibilities at low temperatures and increasing susceptibility with increasing temperature above 50 K are characteristic of a diamagnetic cluster ground state and internal antiferromagnetic coupling between iron sites; the minimum and the rising susceptibility at very low temperatures is indicative of trace paramagnetic contamination. The odd-electron cluster **3** exhibits susceptibility behavior that follows the linear Curie−Weiss law ($\chi^M = C/(T-\theta)$; $C = 0.54$ emu K/mol, $\theta = -4.2$ K) at temperatures below 60 K, but deviates toward higher spin values as temperature increases (Figure 4); this is consistent with an antiferromagnetically

(31) Cleland, W. E.; Holtman, D. A.; Sabat, M.; Ibers, J. A.; DeFotis, G. C.; Averill, B. A. *J. Am. Chem. Soc.* **1983**, *105*, 6021.
(32) (a) Laskowski, E. J.; Frankel, R. B.; Gillum, W. O.; Papaefthymiaou, G. C.; Renaud, J.; Ibers, J. A.; Holm, R. H. *J. Am. Chem. Soc.* **1978**, *100*, 5322. (b) Herskovitz, T.; Averill, B. A.; Holm, R. H.; Ibers, J. A.; Phillips, W. D.; Weiher, J. F. *Proc. Natl. Acad. Sci. U.S.A.* **1972**, *69*, 2437.

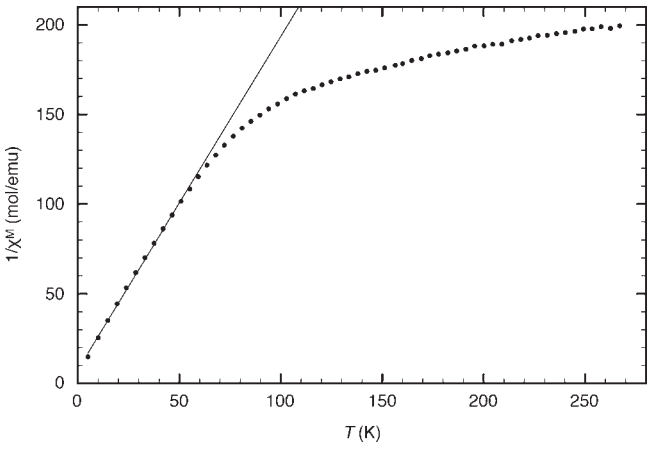

Figure 4. Temperature dependence plot of the reciprocal magnetic susceptibility of polycrystalline $[Na(THF)_2][Fe_4S_4(N\{SiMe_3\}_2)_4]$ (**3**). The solid line indicates the linear least-squares fit ($1/\chi^M = (T - \theta)/C$; $C = 0.54$ emu K/mol, $\theta = -4.2$ K) to the data between $T = 4-55$ K.

coupled, $S' = 1/2$ system (ideal spin-only $C = 0.375$ emu K/mol, assuming $g = 2.0$), with thermal population of excited state spin manifolds.

^{57}Fe Mössbauer spectra collected with zero applied magnetic field at 4.2 K exhibit single quadrupole doublets for clusters **2**, **3**, and **4**; all data were fit as symmetric doublets (Table 7), and the spectra are included as Supporting Information. The actual doublet for **4** is slightly asymmetric, perhaps reflecting the site-differentiation arising from the cation-cluster interactions in the solid-state structure. The spectrum of cluster **3** also shows asymmetric absorptions, and these are broader relative to those of the other clusters under identical measurement conditions; at 150 K, the features sharpen to yield line shapes that can be fit as two symmetric doublets in a 1:1 ratio. These observations are consistent with temperature-dependent relaxation behavior, and, as in **4**, cation-associated site-differentiation in **3** could account for the presence of two doublets at the higher temperature. The isomer shifts of the FeS_3N coordination spheres in the present clusters are slightly lower than typical values associated with tetrahedral FeS_4 environments at the same mean oxidation states.[20a]

Conclusion

The three members of the redox series $[Fe_4(\mu_3\text{-}S)_4(N\{SiMe_3\}_2)_4]^z$ ($z = 0, 1-, 2-$) are readily prepared by the reaction of $FeCl(N\{SiMe_3\}_2)_2(THF)$ with NaSH, followed by reduction with Na_2S as needed. The bis(trimethylsilyl)amide ligand is receiving increasing application in the context of Fe−S chemistry, but the effects of this ligand environment, and, more broadly, those of N-anion donors in general, on Fe−S chemistry have yet to be analyzed in detail. We summarize here the principal characteristics of bis(trimethylsilyl)amide as a terminal ligand on the $[Fe_4S_4]$ cubane core:

(1) Bis(trimethylsilyl)amide ligation affects the cluster core most prominently in its redox potentials, conferring enhanced oxidative stability relative to all other previously studied weak-field terminal ligand types. This stabilization allows facile access to the $[Fe_4S_4]^{4+,3+}$ core oxidation states; for synthetic weak-field $[Fe_4S_4]$ systems with monodentate terminal ligands, the $[Fe_4S_4]^{3+}$ state has been isolated in only one prior instance, while the $[Fe_4S_4]^{4+}$ state is unique to the present amide-ligated system. The intrinsic donor capacity of the N-anion accounts for the thermodynamic stabilization of higher oxidation states; in addition, the steric shielding provided by the amide substituents and the resistance of the amide ligand to oxidative decomposition probably contribute to the stability of the oxidized clusters as well. Redox effects are also evident in the electronic absorption spectrum of **4**, which shows blue-shifted LMCT transitions relative to isoelectronic thiolate and aryloxide systems.

(2) The steric demand of the bis(trimethylsilyl)amide ligand set appears to compress S−Fe−S bond angles, with associated changes in Fe···Fe and S···S core distances. Although this effect is evident when comparing relevant metrics, the net impact on the overall cubane structure is limited. The cubane core is also relatively unaffected by changes in redox state, even as the terminal iron-amide bond lengths increase progressively with reduction. The structures of the sodium salts of the monoanion and dianion are notable in the unique tight association of each individual cation with a cluster core sulfide and an adjacent amide nitrogen.

Experimental Section

General Considerations. Previously described anaerobic synthetic and analytical (cyclic voltammetry; ^{1}H NMR, UV−vis, Mössbauer spectroscopies; elemental analyses) protocols[15] were used in the present study. Magnetic measurements were obtained using a Quantum Design Model 6000 Physical Property Measurement System on finely ground, polycrystalline samples; the magnetic data were corrected for diamagnetism using tabulated Pascal's constants.[33] $FeCl(N\{SiMe_3\}_2)_2(THF)$ (**1**)[15b] was prepared by literature method; all other chemicals were obtained from commercial sources.

$Fe_4S_4(N\{SiMe_3\}_2)_4$ (2). A solution of $NaN(SiMe_3)_2$ (1.134 g, 6.2 mmol) in 10 mL of THF was added slowly to a rapidly stirred solution suspension of $FeCl_3$ (0.500 g, 3.1 mmol) in 35 mL of THF, resulting in an immediate color change to a deep red-black. After 2 h, solid NaSH (0.174 g, 3.1 mmol) was added, resulting in a gradual color change to deep black. Stirring was continued for 8 h, after which the solution was filtered through diatomaceous earth (Celite) and evaporated to dryness in vacuo. The black residue was dissolved in *n*-pentane (60 mL), which was then filtered, concentrated to 25 mL, and held for 12 h at −33 °C to give crystals of **3**. After removing this crystalline contaminant, the filtrate was concentrated to 10 mL and allowed to stand for an additional 12 h at −33 °C. At this point, the solution yielded no additional **3**, and its NMR spectrum revealed only the presence of neutral **2**. The solution was reduced to a final volume of 1 mL and charged with 7 mL of hexamethyldisiloxane (HMDS). After standing at −33 °C for 72 h, large black crystals (210 mg) were isolated and washed with cold HMDS. A second crystalline crop (45 mg) was obtained by evaporating the mother liquor to dryness and resetting the *n*-pentane/HMDS crystallization. Total yield: 255 mg (33% based on $FeCl_3$). Anal. Calcd for $C_{24}H_{72}N_4S_4Si_8Fe_4$: C, 29.02; H, 7.31; N, 5.64. Found: C, 28.87; H, 6.98; N, 5.53.

$[Na(THF)_2][Fe_4S_4(N\{SiMe_3\}_2)_4]$ (3). The procedure for the preparation of **2** was followed up to the addition of NaSH at the following scale: 2.268 g of $NaN(SiMe_3)_2$ (12.4 mmol) in 15 mL of THF; 1.00 g of $FeCl_3$ (6.2 mmol) in 100 mL of THF; 0.347 g of NaSH (6.2 mmol). After stirring the mixture for 8 h, Na_2S (0.120 g, 1.5 mmol) was added as a suspension in THF (10 mL).

(33) Hellwege, K. H.; Hellwege, A. M. *Diamagnetic Susceptibility*; Madelung, O., Ed.; Springer Verlag: New York, 1986; Vol. *16*. This reference gives no correction for the Me_3Si group, so this value was extrapolated from other entries in the table. Correction factors used: **2**, 546.6×10^{-6} emu/mol; **3**, 657.5×10^{-6} emu/mol; **4**, 768.4×10^{-6} emu/mol.

Table 8. Crystallographic Data for $Fe_4S_4(N\{SiMe_3\}_2)_4$ (**2**), $[Na(THF)_2][Fe_4S_4(N\{SiMe_3\}_2)_4]$ (**3**), $[Na(THF)_2]_2[Fe_4S_4(N\{SiMe_3\}_2)_4]$ (**4**), and $[Li(THF)_4][Fe_4S_4(N\{SiMe_3\}_2)_4]$ (**5**)[a]

	2	**3**	**4**	**5**
formula	$C_{24}H_{72}Fe_4N_4S_4Si_8$	$C_{32}H_{88}Fe_4N_4NaO_2S_4Si_8$	$C_{40}H_{104}Fe_4N_4Na_2O_4S_4Si_8$	$C_{40}H_{104}Fe_4LiN_4O_4S_4Si_8$
fw	993.22	1160.41	1327.61	1288.57
space group	$P2_1/c$ (no. 14)	$P2_1/c$ (no. 14)	$P2_1/n$ (no. 14)	$P\bar{4}2_1c$ (no. 114)
Z	4	4	4	2
a, Å	14.9406(6)	12.3146(5)	24.1957(6)	12.7066(7)
b, Å	12.5027(5)	21.7116(8)	11.7829(4)	12.7066(7)
c, Å	27.2026(8)	22.7562(10)	24.7025(9)	21.6126(14)
β, deg	97.901(2)	96.6050(13)	96.766(2)	
V, (Å^3)	5033.1(3)	6043.9(4)	6993.5(4)	3489.5(4)
ρ_{calc}, g/cm^3	1.311	1.275	1.261	1.226
θ_{max}, deg	22.98	27.46	21.99	23.98
total data,[b] %	99.9	99.9	99.4	100.0
μ, mm^{-1}	1.507	1.274	1.117	1.106
R_1 (wR_2),[c] %	4.30 (9.72)	4.96 (9.72)	5.76 (13.41)	4.68 (9.04)
S[d]	1.016	1.017	1.049	1.040

[a] Data collected at $T = 200(2)$ K using Φ and ω scans with graphite-monochromatized Mo Kα radiation ($\lambda = 0.71073$ Å). [b] Percent completeness of (unique) data collection within the θ_{max} limit. [c] Calculated for $I > 2\sigma(I)$: $R_1 = \sum||F_o| - |F_c||/\sum|F_o|$, $wR_2 = \{\sum w(F_o^2 - F_c^2)^2/\sum w(F_o^2)^2\}^{1/2}$. [d] S = goodness of fit = $\{\sum[w(F_o^2 - F_c^2)^2]/(n-p)\}^{1/2}$, where n is the number of reflections and p is the number of parameters refined.

After an additional 8 h, the solution was filtered through diatomaceous earth, and the filtrate evaporated to dryness. The resulting residue was dissolved in *n*-pentane (80 mL), which was filtered, concentrated to 30 mL, and charged with HMDS (10 mL). After further concentration to 20 mL, an additional 5 mL of HMDS was added. A final volume reduction to 15 mL yielded copious microcrystalline product. The mixture was held at −33 °C for 12 h, then filtered to isolate the crystalline solid, which was washed with cold HMDS (5 mL) and dried in vacuo for 4 h. Total yield: 993 mg (56% based on $FeCl_3$). Anal. Calcd for $C_{24}H_{72}N_4NaS_4Si_8Fe_4 \cdot 2C_4H_8O$: C, 33.12; H, 7.64; N, 4.80. Found: C, 32.97; H, 7.34; N, 4.70.

$[Na(THF)_2]_2[Fe_4S_4(N\{SiMe_3\}_2)_4]$ (4). The procedure for the preparation of **2** was followed up to the addition of NaSH at the following scale: 0.567 g of $NaN(SiMe_3)_2$ (3.1 mmol) in 10 mL of THF; 0.250 g of $FeCl_3$ (1.55 mmol) in 20 mL of THF; 0.087 g of NaSH (1.55 mmol). After stirring the mixture for 8 h, Na_2S (0.120 g, 1.5 mmol) was added as a suspension in 10 mL of THF. After an additional 8 h, the solution was filtered through diatomaceous earth and the filtrate evaporated to dryness. The resulting residue was extracted into *n*-pentane (200 mL), which was then filtered, concentrated to 85 mL, and held at −33 °C for 36 h. The crystalline product was isolated and washed with cold *n*-pentane (5 mL). Yield: 204 mg (40% based on $FeCl_3$). Anal. Calcd for $C_{24}H_{72}N_4Na_2S_4Si_8Fe_4 \cdot 4C_4H_8O$: C, 36.12; H, 7.90; N, 4.22. Found: C, 36.27; H, 7.83; N, 4.07.

$[Li(THF)_4][Fe_4S_4(N\{SiMe_3\}_2)_4]$ (5). A mixture of **1** (0.242 g, 0.50 mmol) and LiCl (0.021 g, 0.50 mmol) was stirred in THF (15 mL) overnight. The resulting dark orange-red solution was then added to a suspension of Li_2S (0.012 g, 0.25 mmol) in THF (15 mL), and the mixture heated at 80 °C overnight. The dark brown-red solution was filtered and concentrated to a brown oil in vacuo. The oil was dissolved in *n*-pentane, then cooled to −30 °C to yield a small number of crystals as well as a brown tar. The crystals were identified by X-ray diffraction analysis as **5**. ^{1}H NMR analysis of the precipitated mixture showed the presence of a number of species, with the dominant resonances assignable as signals for **2** and the cluster anion of **3**.

X-ray Crystallography. Single crystals suitable for X-ray diffraction analysis were obtained by storage of *n*-pentane/HMDS (**2** as black blocks; **3** as brown-black parallelpipeds) or *n*-pentane solutions (**4** as yellow-black parallelpipeds; **5** as black plates) at about −30 °C.

General crystallographic procedures are detailed elsewhere.[34] ψ-scan absorption corrections were applied using the Siemens SHELXTL software suite,[35] and multiscan absorption corrections were applied using PLATON.[36] Appropriate disorder models and restraints were employed as needed. Essential crystallographic data for the compounds in this work are summarized in Table 8, with specific details for individual structure determinations available as Supporting Information.

Acknowledgment. This research was supported by the Arnold and Mabel Beckman Foundation (Beckman Young Investigator Award), the U.S. National Science Foundation (CAREER CHE-9984645), and NSERC. C.R.S. thanks the Summer Undergraduate Research Program of Princeton University for funding. We thank Prof. R. Cava and Dr. T. Klimczuk (Princeton) for assistance with magnetochemical measurements, Prof. C. Achim (Carnegie-Mellon) for helpful discussions and experimental assistance, and Prof. R. H. Holm (Harvard) for access to a Mössbauer spectrometer.

Supporting Information Available: Crystallographic, NMR, magnetochemical, and Mössbauer data. This material is available free of charge via the Internet at http://pubs.acs.org.

(34) Kayal, A.; Ducruet, A. F.; Lee, S. C. *Inorg. Chem.* **2000**, *39*, 3696.
(35) Sheldrick, G. M. *SHELXTL*, Version 5.04; Siemens Analytical X-ray Instruments: Madison, WI, 1996.
(36) Spek, A. L. *Acta Crystallogr., Sect. A: Found. Crystallogr.* **1990**, *46*, C34.